

SEPS: SEMANTIC-ENHANCED PATCH SLIMMING FRAMEWORK FOR FINE-GRAINED CROSS-MODAL ALIGNMENT

Xinyu Mao, Junsi Li, Haoji Zhang, Yu Liang, Ming Sun*

School of Computer Science and Engineering
University of Electronic Science and Technology of China
Chengdu, 610065, China

ABSTRACT

Fine-grained cross-modal alignment aims to establish precise local correspondences between vision and language, forming a cornerstone for visual question answering and related multimodal applications. Current approaches face challenges in addressing patch redundancy and ambiguity, which arise from the inherent information density disparities across modalities. Recently, Multimodal Large Language Models (MLLMs) have emerged as promising solutions to bridge this gap through their robust semantic generation capabilities. However, the dense textual outputs from MLLMs may introduce conflicts with the original sparse captions. Furthermore, accurately quantifying semantic relevance between rich visual patches and concise textual descriptions remains a core challenge. To overcome these limitations, we introduce the Semantic-Enhanced Patch Slimming (SEPS) framework, which systematically addresses patch redundancy and ambiguity. Our approach employs a two-stage mechanism to integrate unified semantics from both dense and sparse texts, enabling the identification of salient visual patches. Additionally, it leverages relevance-aware selection with mean value computation to highlight crucial patch-word correspondences, thereby improving cross-modal similarity assessment. Comprehensive experiments on Flickr30K and MS-COCO datasets validate that SEPS achieves superior performance, surpassing existing approaches by 23%-86% in rSum across diverse model architectures, with notable enhancements in text-to-image retrieval scenarios. Our implementation is available at <https://github.com/Sweet4tars/seps.git>.

1 INTRODUCTION

Fine-grained cross-modal alignment between vision and language has emerged as a cornerstone for establishing precise local correspondences across modalities, serving as the foundation for visual question answering (Guo et al., 2019), image captioning (Li et al., 2019), and cross-modal retrieval (Fu et al., 2023). As multimodal applications demand increasingly sophisticated understanding capabilities, achieving accurate alignment between visual patches and semantic concepts has become critical for advancing the field.

Despite this importance, existing cross-modal alignment methods universally face the fundamental challenge of bridging the information gap between modalities. This gap stems from the contrasting nature of cross-modal information representation: visual inputs provide dense, continuous spatial information, while textual descriptions offer sparse, discrete semantic anchors that capture only salient scene aspects. With Vision Transformer (ViT) based models (Dosovitskiy et al., 2020) becoming mainstream through efficient patch-based image processing in fine-grained alignment methods, this information gap manifests itself as two problems: patch redundancy, where numerous visual patches contain overlapping or irrelevant information with no explicit textual counterparts, and patch ambiguity, where sparse textual elements are difficult to map reliably to individual patches. These problems particularly impair text-to-image retrieval performance in complex visual scenarios. As

*Corresponding author: sunm@uestc.edu.cn

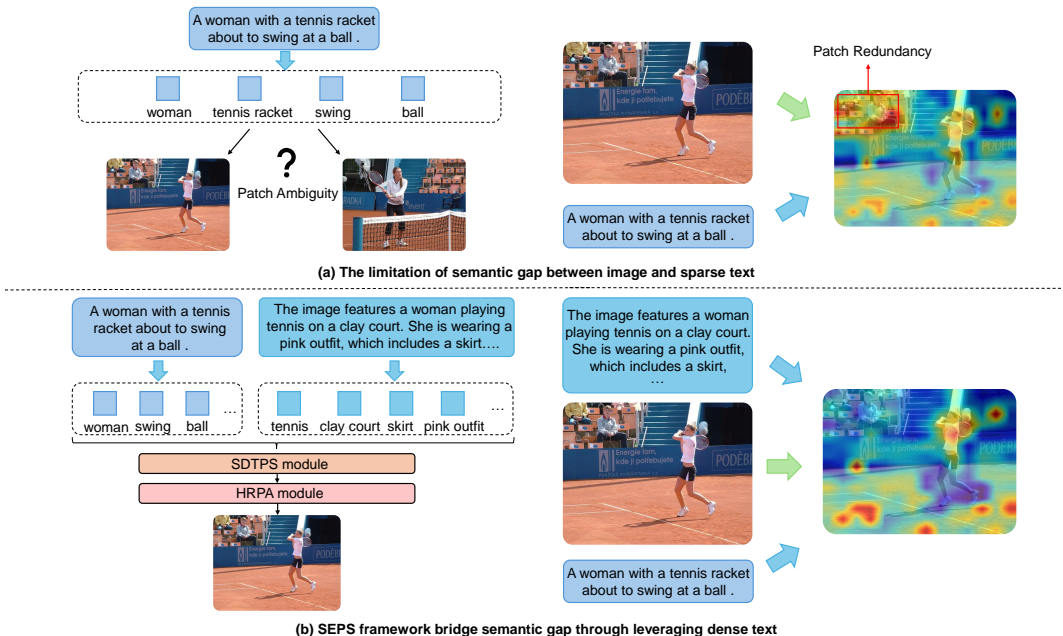


Figure 1: The motivation of our framework, where blue arrows mean language transformer, and green arrows mean vision transformers. (a) Current works suffer from patch ambiguity and patch redundancy due to the limited semantic guidance. (b) Our framework fuses unified semantics derived from dense and sparse texts to guide visual patch selection, and introduces a relevance-aware selection to improve patch-word alignment, which bridges the semantic gap.

illustrated in Figure 1(a), generic captions such as "A woman with a tennis racket about to swing at a ball" lack distinctive visual descriptors, highlighting this inherent information density disparity.

Recently, Multimodal Large Language Models (MLLMs) have emerged as promising solutions to bridge this semantic gap through their robust semantic generation capabilities (Pan et al., 2023; Fu et al., 2024; Liu et al., 2025a). However, MLLM integration introduces semantic inconsistencies, as comprehensive MLLM-generated descriptions may conflict with existing concise captions, potentially causing confusion in cross-modal alignment and degrading retrieval performance. Additionally, accurately quantifying semantic relevance between rich visual patches and concise textual descriptions remains challenging, as conventional alignment methods rely on global averaging, failing to recognize that only a subset of patches are semantically relevant, thus allowing irrelevant regions with low similarity scores to dilute the overall alignment quality.

To overcome these limitations, we introduce the Semantic-Enhanced Patch Slimming (SEPS) framework, which systematically addresses both patch redundancy and ambiguity through strategic MLLM integration, as shown in Figure 1(b). Our key insight centers on employing a two-stage mechanism that integrates unified semantics derived from both dense MLLM-generated texts and sparse original captions, where dense texts provide contextual guidance while sparse texts serve as specific queries for salient patch identification.

Specifically, as illustrated in Figure 2(a), our framework operates through a comprehensive pipeline: we first extract visual patches alongside sparse-text and dense-text feature representations, then aggregate semantically selected visual patches through Sparse and Dense Text-Aware Patch Selection (SDTPS) module, which makes informed selection decisions based on complementary textual perspectives. Finally, we employ our Highly-Relevant Patch-Word Alignment (HRPA) module with relevance-aware selection and mean value computation to facilitate nuanced fine-grained interactions, amplifying highly-relevant patch-word correspondences and improving alignment quality.

The contributions of this paper are as follows:

- To the best of our knowledge, we propose the first systematic framework that strategically employs MLLMs to assist visual patch selection for cross-modal alignment, addressing fundamental patch redundancy and ambiguity challenges.
- We introduce a novel two-stage mechanism that incorporates unified semantic representations derived from both dense and sparse textual modalities. This mechanism eliminates potential semantic inconsistencies, enabling more accurate identification of salient visual patches.
- We develop a relevance-aware selection mechanism augmented by mean value calculation, which enhances the emphasis on critical patch-word correspondences. This design effectively mitigates the averaging bias inherent in traditional methods and improves cross-modal similarity evaluation.
- We achieve superior performance on Flickr30K and MS-COCO datasets, surpassing existing approaches by 23%-86% in rSum across diverse model architectures, with notable enhancements in text-to-image retrieval scenarios.

2 RELATED WORK

2.1 CROSS-MODAL ALIGNMENT

Cross-modal alignment aims to bridge the semantic gap between vision and language through two primary strategies: coarse-grained and fine-grained alignment. Coarse-grained methods, such as VSE++ (Faghri et al., 2017), compute the global similarity between an entire image and a text. In contrast, fine-grained methods achieve more precise matching by modeling interactions between local features, such as specific image regions and individual words. Early approaches relied on object detectors like Faster R-CNN (Girshick, 2015) to extract visual regions, followed by cross-attention mechanisms for alignment, as seen in SCAN (Lee et al., 2018), SGR (Diao et al., 2021), and CHAN (Pan et al., 2023). However, this paradigm is computationally expensive, its performance is dependent on the detector’s accuracy, and it is prone to error propagation. Recently, end-to-end models based on the Vision Transformer (ViT) (Dosovitskiy et al., 2020) have become mainstream. ViT processes images by dividing them into patches, but this introduces new challenges: patch redundancy and patch ambiguity. To mitigate these problems, recent work like LAPS (Fu et al., 2024) demonstrates the potential of using linguistic supervision to prune redundant patches by leveraging captions from standard datasets. While effective, the semantic sparsity inherent in these captions creates a performance bottleneck, particularly in complex visual scenarios. Building on this foundation, our work addresses this bottleneck by integrating dense semantic guidance with the original sparse text, exploring how this hybrid supervision can unlock further improvements in patch selection.

2.2 INFORMATION DENSITY AND DENSE TEXT SUPERVISION

Visual signals are dense, while textual descriptions are relatively sparse, leading to a fundamental information capacity mismatch. This challenge has motivated a significant recent trend: the use of Multimodal Large Language Models (MLLMs) to generate dense text, which provides a much richer supervisory signal to bridge this gap. Several works have begun to leverage this rich data. One line of research focuses on enhancing a model’s general long-text capabilities through pre-training, such as in LongCLIP (Zhang et al., 2024) and LoTLIP (Wu et al., 2024). Other approaches tackle the density mismatch at the feature representation level. For instance, methods learn diverse embedding sets (e.g. PCME (Chun et al., 2021)) or design asymmetric architectures (e.g. AVSE (Liu et al., 2025c)) to accommodate modal differences, while the prominent D2S-VSE (Liu et al., 2025b) uses dense text as a “teacher” signal to distill knowledge and enrich sparse text representations.

However, a common thread unites these existing methods: they primarily optimize at the feature representation or alignment stage—either by improving the model’s global understanding or by enhancing the textual representations. The granular semantic details within dense text have not been exploited to directly address visual information redundancy at the input level. Therefore, our work explores how to leverage this fine-grained information to directly guide the visual patch selection process, aiming to solve the information mismatch by proactively refining the visual input itself.

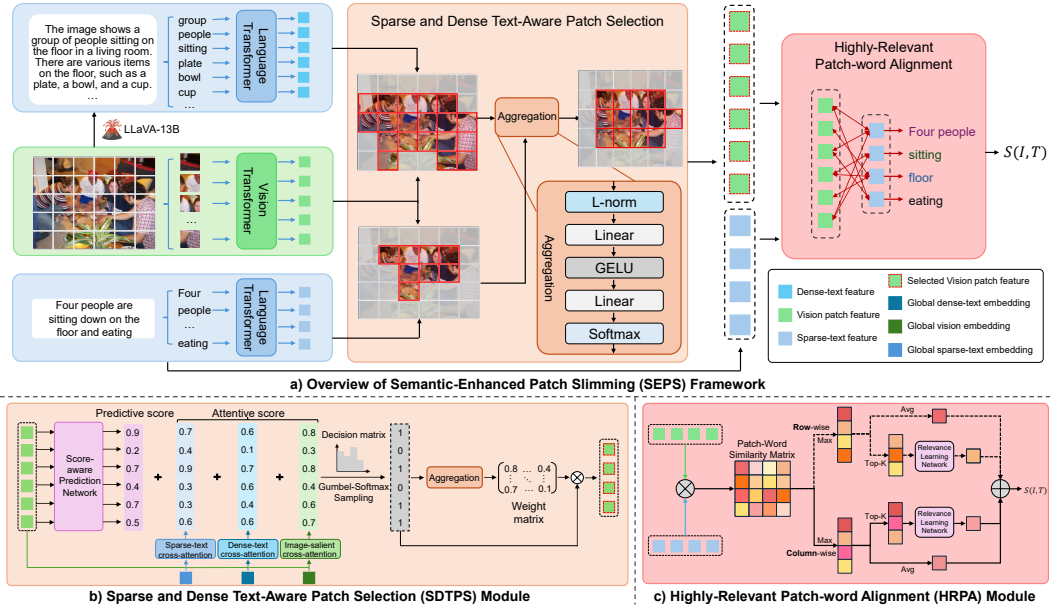


Figure 2: (a) Overview of our Semantic-Enhanced Patch Slimming(SEPS) Framework for fine-grained cross-modal alignment. Given an image-text pair (I, T) , we first use pure Transformer encoders to extract visual patch features and textual word features. Then, we propose the SDTPS module to identify text-relevant patches under the support of dense text generated by MLLMs. Finally, we propose the HRP module to compute the patch-word alignment score $S(I, T)$. (b)(c) The detailed architecture of the proposed SDTPS and HRP modules, respectively.

3 METHODOLOGY

This section introduces the SEPS framework, which integrates dense textual representations generated by MLLMs with original sparse textual features through a novel two-stage mechanism. Coupled with a relevance-aware mechanism, the framework effectively addresses semantic inconsistency in large model integration and similarity shift bias in existing alignment computation, thereby bridging the semantic gap between visual and textual modalities and resolving patch redundancy and ambiguity issues prevalent in current alignment methodologies. The framework architecture encompasses three principal modules: the dense text generation component detailed in Section 3.1, the Sparse and Dense Text-Aware Patch Selection Module presented in Section 3.2 and visualized in Figure 2(b), and the Highly-relevant Patch-word Alignment module described in Section 3.3 and illustrated in Figure 2(c).

3.1 DENSE TEXT GENERATION BASED ON MLLMS

To generate dense textual representations for visual inputs, we employ the pre-trained multimodal model LLaVa (Liu et al., 2023). For a given input image I , we utilize LLaVa with the instructional prompt "Provide a comprehensive description of this image". The model subsequently generates semantically dense textual output that encodes granular visual information, leveraging its enhanced visual perception capabilities. Implementation details and parameter configurations for LLaVa are specified in Section 4.3. This methodology ensures that the linguistic representation maintains informational richness comparable to the visual modality, thereby mitigating the cross-modal information asymmetry inherent in traditional multimodal systems.

3.2 SPARSE AND DENSE TEXT-AWARE PATCH SELECTION MODULE

The SDTPS module employs a two-stage mechanism to fuse unified semantics derived from dense and sparse texts, thereby identifying visual patches that exhibit robust semantic alignment with such integrated semantic representations. In the first stage, semantic scoring assigns each visual patch a comprehensive score derived from multiple information sources, including sparse textual features,

dense textual features, and intrinsic image characteristics. Subsequently, the second stage employs a decision and aggregation process that utilizes a learned weight matrix to identify and extract the most semantically relevant patches for further alignment.

3.2.1 SEMANTIC SCORING

In first stage, the module employs a score-aware prediction network to assess the semantic relevance of individual visual patches. This network predicts the final scores that each visual patch would obtain from three distinct cross-attention mechanisms, thereby improving the learning capacity of the semantic scoring stage. The network comprises a two-layer MLP followed by a sigmoid activation function.

$$s_i^p = \sigma(\text{MLP}(v_i)), i \in \{1, \dots, N\}, \quad (1)$$

where $s_i^p \in [0, 1]$ represents the significance score for the i -th patch, and $v_i \in V = \{v_1, v_2, \dots, v_N\}$ denotes the visual patch feature vector, σ means sigmoid activation function. A higher value of s_i^p indicates greater semantic significance of the patch v_i .

This prediction network is primarily integrated with attention scores derived from textual content and image self-attention mechanisms to achieve better cross-modal alignment (Meng et al., 2022; Rao et al., 2021). However, given that most text in existing datasets is sparse, an information capacity gap emerges between visual and textual modalities. To address this limitation, we leverage dense text generated by MLLMs to enhance the textual relevance of the significance scores s_i^p for visual patches.

Building upon the cross-attention between visual patches and sparse textual representations, we propose an additional attention mechanism: cross-attention between visual patches and dense textual representations. Therefore, the complete attention score computation formula is as follows:

$$s_i^{st} = \text{Norm}(v_i^T \cdot E_{st}/d) \quad s_i^{dt} = \text{Norm}(v_i^T \cdot E_{dt}/d) \quad s_i^{im} = \text{Norm}(v_i^T \cdot E_{im}/d), \quad (2)$$

where s_i^{st} represents the sparse-text relevance of the visual patch, s_i^{dt} denotes the dense-text relevance of the visual patch, and s_i^{im} represents the significance of the i -th patch in the visual dimension. Norm represents the normalization of attention scores into the $[0, 1]$ range to maintain consistency with the outputs of the prediction network s_i^p . E_{st} , E_{dt} , and E_{im} denote the global embedding vectors of sparse text, dense text, and image, respectively. d is the number of embedding dimensions. Finally the total significance score formula with β as a weight parameter is as follows:

$$s_i = (1 - 2\beta) \cdot s_i^p + \beta \cdot (s_i^{st} + s_i^{dt} + 2s_i^{im}) \quad (3)$$

3.2.2 DECISION AND AGGREGATION

In second stage, the computed significance scores $s = [s_1, s_2, \dots, s_N] \in \mathbb{R}^N$ undergo a binary mapping process through a differentiable decision matrix. Compared to naive sampling approaches, such as selecting the top-K patches, the Gumbel-Softmax technique provides smooth and differentiable sampling capabilities (Maddison et al., 2016). Based on this technique, we follow the previous sampling methodology to obtain differentiable decision matrices D_s and D_d for sparse-text and dense-text, respectively (Fu et al., 2024). D is a one-hot matrix where '1' indicates a significant patch and '0' indicates a redundant patch. Based on the sparse-text matrix D_s and dense-text matrix D_d , we can select significant patches $V_s = \{v_1^s, v_2^s, \dots, v_{N_s}^s\} \in \mathbb{R}^{N_s \times d}$ for sparse-text and $V_d = \{v_1^d, v_2^d, \dots, v_{N_d}^d\} \in \mathbb{R}^{N_d \times d}$ for dense-text.

These binary decisions are subsequently processed through an aggregation network that learns multiple aggregation weights (Zong et al., 2022) and aggregates N_s and N_d significant patches to generate N_c informative patches.

$$\hat{v}_j = \sum_{i=1}^{N_s} (W_s)_{ij} \cdot v_i^s + \sum_{i=1}^{N_d} (W_d)_{ij} \cdot v_i^d, \quad j \in \{1, \dots, N_c\} \quad (4)$$

where $(W_s)_{ij}$ and $(W_d)_{ij}$ are the elements of the normalized weight matrices $W_s \in \mathbb{R}^{N_s \times N_c}$ and $W_d \in \mathbb{R}^{N_d \times N_c}$. N_c is the number of aggregated patches ($N_c < \max(N_s, N_d)$), and we have $\sum_{i=1}^{N_s} (W_s)_{ij} = 1$ and $\sum_{i=1}^{N_d} (W_d)_{ij} = 1$. The weight matrices W_s and W_d are learned by an MLP

followed by a softmax function, taking significant patches based on sparse-text and dense-text as input, respective: $W_s = \text{Softmax}(\text{MLP}(V_s))$ and $W_d = \text{Softmax}(\text{MLP}(V_d))$.

Specifically, we treat the decision matrices D_s and D_d as mask matrices to select the significant patch features V_s and V_d before computing the softmax function. The aggregation network can adaptively aggregate patches with similar semantics and is differentiable for end-to-end training.

3.3 HIGHLY-RELEVANT PATCH-WORD ALIGNMENT

The HRP module introduces relevance-aware selection with mean value computation to facilitate nuanced fine-grained interactions, amplifying highly-relevant patch-word correspondences. As shown in Figure.2(c), we compute the fine-grained alignment by the set of selected visual patches \hat{V} and initial sparse textual words T . For convenience, we approximate that $|\hat{V}| = N_c$, $|T| = M$. We first calculate the token-wise similarity to generate the patch-word similarity matrix $A \in \mathbb{R}^{N_c \times M}$, where $A_{ij} = \frac{(\hat{v}_i)^T t_j}{\|\hat{v}_i\| \|t_j\|}$ represents the alignment score between the i -th visual patch and the j -th textual word.

Next, we employ a relevance-aware selection to aggregate the cross-modal alignment, which enhances the contribution of maximally relevant patch-word pairs to image-text similarity, thereby improving alignment quality. We identify the most aligned textual token (or visual patch) for each visual patch (or textual token), and use the relevant learning network to transform the selected maximum scores into a scalar value. Then calculate the average of total aligned scores. The sum of these two values represent the overall alignment score between the image I and the sentence T , denoted $S(I, T)$.

$$\begin{aligned}
 S(I, T) = & \underbrace{\left(\frac{1}{N_c} \sum_{i=1}^{N_c} \max_j(A)_{ij} + \text{MLP}(\text{TOPK}(\max_j(A)_{ij})) \right)}_{\text{patch-to-word alignment}} \\
 & + \underbrace{\left(\frac{1}{M} \sum_{j=1}^M \max_i(A)_{ij} + \text{MLP}(\text{TOPK}(\max_i(A)_{ij})) \right)}_{\text{word-to-patch alignment}}
 \end{aligned} \tag{5}$$

Following prior work, we adopt a bidirectional triplet loss with hard negative mining(Faghri et al., 2017):

$$\begin{aligned}
 \mathcal{L}_{\text{align}} = & \sum_{(I, T)} \left(\left[\alpha - S(I, T) + S(I, \hat{T}) \right]_+ \right. \\
 & \left. + \left[\alpha - S(I, T) + S(\hat{I}, T) \right]_+ \right)
 \end{aligned} \tag{6}$$

where α is the margin, $[x]_+ = \max(x, 0)$, and (I, T) denotes a positive image-text pair within the mini-batch. The hardest negatives are defined as $\hat{T} = \arg \max_{j \neq T} S(I, j)$ and $\hat{I} = \arg \max_{i \neq I} S(i, T)$ for text and image, respectively.

Furthermore, to enhance training stability, we constrain the proportion of selected patches to a target value ρ (Rao et al., 2021), and supervise this constraint using mean-squared-error losses computed from the sparse-text and dense-text views, respectively. Finally, we combine the cross-modal alignment loss $\mathcal{L}_{\text{align}}$ Eq.6 with the ratio constraint loss $\mathcal{L}_{\text{ratio}}$:

$$\begin{aligned}
 \mathcal{L}_{\text{ratio}} = & \left(\rho - \lambda_1 \cdot \frac{1}{N_s} \sum_{i=1}^{N_s} (D_s)_i - \lambda_2 \cdot \frac{1}{N_d} \sum_{i=1}^{N_d} (D_d)_i \right)^2, \\
 \mathcal{L} = & \mathcal{L}_{\text{align}} + \mathcal{L}_{\text{ratio}}
 \end{aligned} \tag{7}$$

where λ_1 and λ_2 are constant coefficients for sparse text and dense text.

Table 1: Comparisons of image-text retrieval performances on Flickr30K and MS-COCO test-set. We list the details of feature encoding, image resolution, and the number of obtained regions/patches by visual encoder (e.g. “ViT-Base-224” represents the base-version of Vision Transformer with 224×224 image resolution input, regarding 16×16 pixels as one patch, and getting 14×14 visual patches for one image). FG indicates whether it is the fine-grained cross-modal alignment. The best results are marked **bold**, and the second best results are marked underline.

Method	FG	Flickr30K 1K						MS-COCO 1K						MS-COCO 5K								
		Image-to-Text R@1 R@5 R@10	Text-to-Image R@1 R@5 R@10	rSum	Image-to-Text R@1 R@5 R@10	Text-to-Image R@1 R@5 R@10	rSum	Image-to-Text R@1 R@5 R@10	Text-to-Image R@1 R@5 R@10	rSum												
<i>ViT-Base-224 + BERT-base, 14×14 patches</i>																						
VSE++ (Faghri et al., 2017)	✗	71.8	92.8	96.5	59.4	84.7	90.9	496.1	75.0	94.6	98.0	62.7	89.4	94.9	514.6	52.4	80.3	88.8	40.6	70.4	81.1	413.4
SCAN (Lee et al., 2018)	✓	69.5	90.9	95.6	56.4	83.1	90.0	485.6	76.0	95.4	98.1	64.5	90.8	95.8	520.6	53.9	81.8	90.0	42.9	72.3	82.5	423.5
SGR (Diao et al., 2021)	✓	69.7	90.8	95.2	59.1	84.1	89.9	488.7	77.2	95.0	98.0	65.1	90.7	95.8	521.8	54.9	82.8	90.5	42.8	72.2	82.5	425.8
CHAN (Pan et al., 2023)	✓	69.2	91.8	95.0	58.4	84.9	90.6	489.9	77.1	95.1	98.1	65.0	91.0	96.0	522.2	56.3	83.2	90.1	43.0	72.6	82.8	428.0
LAPS (Fu et al., 2024)	✓	74.0	93.4	97.4	62.5	87.3	92.7	507.3	78.7	95.5	98.3	66.2	91.3	96.2	526.3	57.5	84.0	90.8	44.5	74.0	83.6	434.4
AVSE (Liu et al., 2025c)	✗	76.0	<u>94.6</u>	<u>97.5</u>	62.7	88.4	93.1	512.3	79.8	<u>95.6</u>	<u>98.3</u>	67.0	91.5	96.3	528.5	58.8	84.3	91.0	45.1	74.3	83.9	437.4
D2S-VSE (Liu et al., 2025b)	✗	82.8	96.1	98.3	<u>68.5</u>	<u>91.3</u>	<u>94.9</u>	<u>531.9</u>	80.1	97.0	99.2	<u>68.1</u>	<u>92.5</u>	<u>96.7</u>	<u>533.7</u>	<u>60.1</u>	85.5	92.5	<u>46.3</u>	<u>75.9</u>	<u>85.2</u>	<u>445.6</u>
SEPS	✓	86.1	93.7	96.9	86.9	98.1	99.2	560.9	89.0	94.8	98.0	88.5	99.3	99.8	569.5	73.9	<u>85.2</u>	<u>92.1</u>	73.5	94.5	97.8	516.9
<i>ViT-Base-384 + BERT-base, 24×24 patches</i>																						
VSE++ (Faghri et al., 2017)	✗	77.1	95.7	97.5	65.8	90.2	94.3	520.5	77.0	95.7	98.4	64.6	91.1	96.2	523.0	54.9	82.8	90.4	42.4	72.4	82.8	425.8
SCAN (Lee et al., 2018)	✓	75.4	94.4	96.9	63.6	88.6	93.5	512.5	76.1	95.5	98.5	65.1	91.6	96.3	523.1	53.3	81.8	90.0	42.6	72.6	82.9	423.1
SGR (Diao et al., 2021)	✓	76.9	94.9	98.1	64.2	88.4	93.3	515.8	75.8	95.7	98.6	65.6	92.0	96.5	524.2	53.3	81.0	89.6	42.9	73.1	83.7	423.6
CHAN (Pan et al., 2023)	✓	75.4	94.5	97.6	63.2	88.6	93.1	512.4	78.1	95.8	98.6	66.1	92.1	96.6	527.3	55.6	83.8	91.2	43.4	73.6	83.5	431.1
LAPS (Fu et al., 2024)	✓	79.0	96.0	98.1	67.3	90.5	94.5	525.4	78.6	96.3	98.9	68.0	92.4	96.8	531.0	57.4	84.9	92.5	46.4	75.8	85.2	442.2
AVSE (Liu et al., 2025c)	✗	80.3	<u>96.4</u>	<u>98.7</u>	67.9	91.2	94.7	529.2	<u>81.1</u>	<u>97.1</u>	<u>99.0</u>	68.3	92.7	<u>97.0</u>	<u>535.2</u>	<u>61.2</u>	<u>86.8</u>	<u>93.2</u>	46.2	75.9	85.0	448.3
D2S-VSE (Liu et al., 2025b)	✗	<u>84.1</u>	97.5	99.1	<u>70.3</u>	<u>91.6</u>	<u>95.3</u>	<u>537.9</u>	80.8	97.2	99.1	<u>69.0</u>	<u>92.9</u>	96.8	<u>535.8</u>	60.6	86.5	93.2	<u>46.8</u>	<u>76.4</u>	<u>85.7</u>	<u>449.1</u>
SEPS	✓	90.7	94.4	98.4	89.3	99.3	99.5	571.5	90.9	96.1	98.8	91.0	99.5	99.8	576.1	77.8	88.7	94.8	78.5	96.3	98.7	534.6
<i>Swin-Base-224 + BERT-base, 7×7 patches</i>																						
VSE++ (Faghri et al., 2017)	✗	82.5	96.5	98.9	70.0	91.4	95.1	534.4	83.3	97.5	99.3	71.0	93.0	96.7	540.9	64.0	88.2	94.2	49.9	78.0	86.6	460.9
SCAN (Lee et al., 2018)	✓	79.0	95.9	98.2	67.7	90.6	94.9	526.3	80.9	97.0	<u>99.1</u>	69.7	93.1	97.1	536.9	60.7	86.6	93.2	48.1	77.1	86.1	451.8
SGR (Diao et al., 2021)	✓	80.4	97.0	98.7	66.9	90.2	94.5	527.6	81.2	97.1	99.1	69.9	93.2	97.2	537.7	61.0	86.7	93.2	48.6	77.2	86.3	453.1
CHAN (Pan et al., 2023)	✓	81.4	97.0	98.6	68.5	90.6	94.5	530.6	81.6	97.2	99.3	70.6	93.7	<u>97.6</u>	539.8	64.1	87.9	93.5	49.1	77.3	86.1	458.0
LAPS (Fu et al., 2024)	✓	82.4	<u>97.4</u>	<u>99.5</u>	70.0	91.7	95.4	536.3	84.0	<u>97.6</u>	99.3	<u>72.1</u>	93.7	97.3	544.1	64.5	<u>89.2</u>	<u>94.4</u>	41.6	78.9	87.2	465.8
AVSE (Liu et al., 2025c)	✗	83.9	97.4	99.4	70.0	92.4	95.6	538.7	<u>84.9</u>	98.0	99.3	72.1	<u>94.0</u>	97.4	<u>545.7</u>	<u>66.2</u>	89.8	94.7	<u>51.7</u>	<u>79.2</u>	87.3	<u>468.9</u>
D2S-VSE (Liu et al., 2025b)	✗	<u>87.2</u>	98.4	99.9	<u>73.0</u>	<u>93.5</u>	<u>96.7</u>	<u>548.7</u>	82.4	97.6	99.3	70.3	93.7	97.4	540.7	63.9	87.7	94.0	49.3	78.3	87.2	460.4
SEPS	✓	89.8	96.9	98.7	88.0	98.9	99.6	572.0	87.2	94.9	98.3	84.7	99.0	99.8	563.9	71.9	86.0	92.4	66.8	92.2	96.8	506.1
<i>Swin-Base-384 + BERT-base, 12×12 patches</i>																						
VSE++ (Faghri et al., 2017)	✗	83.8	97.5	<u>99.2</u>	71.1	93.2	96.2	540.6	82.9	97.7	<u>99.4</u>	71.3	93.5	97.3	542.1	63.0	88.5	94.3	50.1	78.9	87.4	462.2
SCAN (Lee et al., 2018)	✓	81.9	96.9	98.9	70.0	92.7	95.8	536.1	81.6	96.8	99.1	69.1	92.7	96.7	536.1	61.1	87.3	93.3	47.8	76.9	85.9	452.4
SGR (Diao et al., 2021)	✓	80.7	96.8	99.0	69.9	91.7	95.3	533.4	81.9	96.7	99.1	69.3	92.8	96.7	536.6	62.8	87.0	92.9	48.1	77.0	86.0	453.8
CHAN (Pan et al., 2023)	✓	81.2	96.7	98.8	70.3	92.2	95.9	535.0	83.1	97.3	99.2	70.4	93.1	97.1	540.2	63.4	88.4	94.1	49.2	77.9	86.6	459.5
LAPS (Fu et al., 2024)	✓	85.1	97.7	99.2	74.0	93.0	96.3	545.3	84.1	97.4	99.2	<u>72.1</u>	93.9	97.4	544.1	67.1	88.6	94.3	<u>53.0</u>	79.5	87.6	470.1
AVSE (Liu et al., 2025c)	✗	87.1	<u>98.3</u>	99.2	73.6	93.5	96.5	548.2	<u>85.1</u>	98.2	99.5	71.6	94.0	97.5	<u>545.9</u>	<u>68.6</u>	90.2	95.6	52.2	<u>79.6</u>	87.8	<u>474.0</u>
D2S-VSE (Liu et al., 2025b)	✗	87.8	99.0	99.7	<u>75.7</u>	<u>94.1</u>	<u>96.9</u>	<u>553.2</u>	83.8	<u>97.9</u>	99.4	71.9	<u>94.2</u>	<u>97.9</u>	544.7	65.2	<u>89.2</u>	<u>94.6</u>	51.3	79.4	<u>87.9</u>	467.7
SEPS	✓	93.6	98.3	99.2	91.6	99.4	99.8	581.9	89.5	96.5	99.0	87.1	99.2	99.9	571.2	74.7	88.4	94.3	70.3	93.8	97.6	519.1

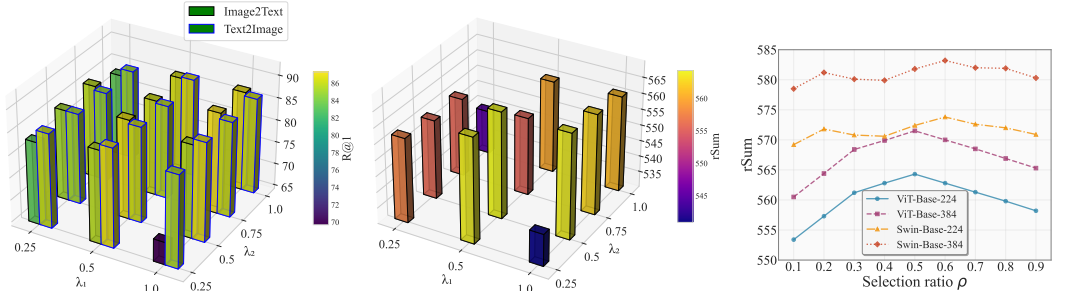


Figure 3: The retrieval performance of different selection ratios ρ , constant coefficients λ_1 and λ_2 with various visual encoders on Flickr30K.

4 EXPERIMENTS

4.1 DATASETS

Following prior works (Diao et al., 2021; Faghri et al., 2017; Lee et al., 2018), we evaluate our model on the widely-used Flickr30K (Young et al., 2014) and MS-COCO (Lin et al., 2014) benchmarks. Each image in these datasets is paired with five textual captions. For Flickr30K, we adopt the standard split of 29,000 training, 1,000 validation, and 1,014 test images. For MS-COCO, we use the common split of 113,287 for training, 5,000 for validation, and 5,000 for testing. We report results on both the 1K test set (averaged over 5 folds) and the full 5K test set.

4.2 METRICS

We adopt Recall@K ($R@K$, $K \in \{1, 5, 10\}$) and rSum as evaluation metrics. $R@K$ measures the percentage of ground truth in the retrieved top-K lists, while rSum aggregates multiple $R@K$ in both directions (image-to-text and text-to-image) to summarize overall retrieval quality.

4.3 IMPLEMENTATION DETAILS

Our code is based on the public code of LAPS (Fu et al., 2024). For dense text generation, we use LLaVa (Liu et al., 2023) to produce detailed textual descriptions. The generation process was configured with a Top-P of 0.9, a temperature of 0.2, and a limit of 500 new tokens. Notably, we treat dense-text generation as an image preprocessing step with no gradients backward. Therefore, no information leakage occurs from the test datasets. For vision encoder, we adopt base-size Vision Transformer (ViT) (Dosovitskiy et al., 2020) (a patch is 16×16 pixels) and Swin Transformer (Swin) (Liu et al., 2021) (a patch is 32×32 pixels). Images are resized to 224×224 or 384×384 , yielding 14×14 and 24×24 patch grids for ViT and 7×7 and 12×12 for Swin. Text is encoded with base-size BERT (Devlin et al., 2019). The whole framework is trained for 30 epochs using AdamW (Loshchilov & Hutter, 2017) optimizer with a batch size of 32 and an initial learning rate of $1e-4$. We use loss with margin $\alpha = 0.2$ and set the constant coefficients $\lambda_1 = \lambda_2 = 1$. For sparsification, we adopt fixed ratios by default: on ViT, selection $\rho = 0.5$; on Swin, selection $\rho = 0.8$.

4.4 COMPARISON WITH STATE-OF-THE-ART METHODS

Following the standard protocols of two benchmarks (Faghri et al., 2017; Zhang et al., 2022), we systematically compare the retrieval performance of SEPS with recent state-of-the-art methods on Flickr30K and MS-COCO. Table 1 details the feature encoders, input resolutions, and whether fine-grained alignment (FG) was adopted for each method. The performance of competing methods is reported directly from their original publications, supplementing with ensemble versions where necessary for comparison. Firstly, we introduce four SOTA cross-modal alignment methods:

- **CHAN (Pan et al., 2023):** Applies a hard-coded selection strategy atop the foundational fine-grained alignment SCAN (Lee et al., 2018), retaining the maximum cross-attention alignment scores.
- **LAPS (Fu et al., 2024):** A fine-grained approach that prunes redundant patches under language guidance, followed by semantic and spatial calibration to enable sparse, bidirectional patch-word alignment.
- **AVSE (Liu et al., 2025c):** A coarse-grained approach that constructs multi-view global image embeddings via radial-biased sampling and performs Asymmetric Embedding Optimal Matching (AEOM) for global alignment.
- **D2S-VSE (Liu et al., 2025b):** A coarse-grained approach that leverages dense-to-sparse distillation with dense captions generated by a multimodal large language model (MLLM) to align cross-modal information capacity, and conducts retrieval via global embedding similarity.

The quantitative results in Table 1 confirm that our SEPS framework sets a new state-of-the-art across all evaluated settings. The core advantage of our framework lies in its ability to dramatically improve text-image retrieval accuracy in large-scale, complex scenes through enhancing textual modal semantic representations and reducing the semantic gap between image and text modalities. Specifically, our approach strengthens the discriminative power of textual features while establishing more precise cross-modal correspondences, enabling better semantic alignment in heterogeneous visual-linguistic spaces. This superiority is most evident on the challenging MS-COCO 5K dataset, where SEPS, using the ViT-Base-224 model, achieves a substantial improvement of 13.8% in Image-to-Text $R@1$ and a massive 27.2% in Text-to-Image $R@1$ compared to the strongest competitor, D2S-VSE. These targeted accuracy gains contribute to an overall rSum improvement of 71.3%. A consistent performance boost is also observed across all backbones on the Flickr30K dataset, demonstrating the robustness of our approach.

Furthermore, to demonstrate the generalizability and robustness of our proposed framework, we extend the SEPS methodology to the widely-adopted pre-trained CLIP model (Radford et al., 2021),

with comprehensive experimental results presented in Appendix Table 3. Additionally, we conduct systematic hyperparameter analysis by visualizing the influence of different hyperparameter configurations on SEPS performance in Figure 3, with corresponding quantitative results detailed in Appendix Table 4 and Table 5. All experimental configurations adhere to the default parameter settings specified in Section 4.3.

4.5 ABLATION STUDY

To systematically evaluate the individual contributions of our key components and assess the parameter sensitivity of our proposed algorithm, we conduct comprehensive ablation studies on the Flickr30K dataset. These experiments examine two core architectural modules and critical hyperparameters, with detailed results presented in Table 2 and Figure 3.

Table 2: Comparison of different module ablations for SEPS framework on Flickr30K. We also show the results of the enhanced textual feature and relevance-aware alignment for our framework

Modules	Different Settings	Image-to-Text		Text-to-Image	
		R@1	R@5	R@1	R@5
SDTPS	only sparse text	78.6	95.1	67.2	90.5
	only dense text	80.3	80.3	80.5	96.8
	without aggregation	85.2	96.1	84.7	97.3
HRPA	only relevance-aware selection	83.3	93.8	82.6	93.9
	only mean value	84.5	94.7	80.1	93.5
	introduce dense-text	84.8	95.7	84.0	96.9
	introduce aggregation	74.4	94.3	62.7	88.3
	introduce relevance-aware selection	74.7	94.8	62.6	88.8
	complete SEPS	86.1	96.7	86.9	98.1

Impact of selection ratios and constant coefficients. As demonstrated in Figure 3, while our framework exhibits robustness in different parameter settings, unbalanced coefficient combinations and excessive or insufficient patch selection slightly affect performance, particularly for ViT-based models.

Effectiveness of unified semantic from dense and sparse texts. As detailed in Table 2, the results decisively validate our central hypothesis regarding the effectiveness of unifying semantic information from both dense and sparse textual modalities. The integration of dense text with sparse text representations in our hybrid framework achieves a remarkable 17.5% improvement in Text-to-Image R@1 performance compared to sparse-text-only baselines. This substantial enhancement demonstrates that the unified semantic understanding is critical for resolving ambiguity in complex visual scenes, thereby validating the fundamental innovation of our framework.

Effectiveness of aggregation. The results show that the inclusion of the aggregation network provides a performance gain of 2.2% in Text-to-Image R@1. This confirms that the aggregation mechanism contributes to the creation of more robust and semantically coherent representations for the final alignment stage.

Effectiveness of relevance-aware selection. A mechanism relying solely on relevance-aware selection reaches at 82.6% in Text-to-Image R@1. However, the complete model reaches a superior 86.9%, confirming our design choice. This performance gain is achieved because mean pooling captures the overall semantic similarity, while relevance-aware selection explicitly rewards the most critical patch-word correspondences, proving that the two strategies are highly complementary.

5 CONCLUSION

In this work, we present the Semantic-Enhanced Patch Slimming (SEPS) framework, a novel approach for fine-grained cross-modal alignment that systematically addresses the fundamental challenges of patch redundancy and semantic ambiguity through strategic integration of MLLMs. The proposed framework introduces two key innovations: the SDTPS module, which resolves semantic conflicts between original sparse textual descriptions and generated dense semantic representations,

and the HRP module, which mitigates the averaging bias introduced by minimal similarity values from irrelevant patches. These complementary modules enable the precise identification of semantically relevant image patches and establish improved patch-word correspondences. Comprehensive experimental evaluation on standard benchmarks, including Flickr30K and MS-COCO datasets, demonstrates that SEPS achieves new state-of-the-art performance across multiple model architectures, yielding substantial improvements of 23%-86% in rSum metrics and establishing its effectiveness for cross-modal retrieval tasks.

ETHICS STATEMENT

In this paper, we use Large Language Models to polish writing in Section 4 and appendix. The dense text used for supervision in our framework is generated by a large pre-trained MLLM. We acknowledge that these models may learn and perpetuate societal biases (e.g. gender and racial stereotypes) from their training data. Consequently, our method risks reinforcing these biases by relying on such models for visual guidance. We recognize this as a significant limitation and a key issue for future research to address.

REPRODUCIBILITY STATEMENT

To improve the reproducibility of our work, we upload our code, including all train logs, evaluate logs and best model checkpoints at <https://anonymous.4open.science/r/SEPS/>. The detailed settings for the hyperparameters are introduced in Section 4.3.

REFERENCES

- Yen-Chun Chen, Linjie Li, Licheng Yu, Ahmed El Kholy, Faisal Ahmed, Zhe Gan, Yu Cheng, and Jingjing Liu. Uniter: Learning universal image-text representations. *arXiv preprint arXiv:1909.11740*, 2019.
- Sanghyuk Chun, Seong Joon Oh, Rafael Sampaio De Rezende, Yannis Kalantidis, and Diane Larlus. Probabilistic embeddings for cross-modal retrieval. In *Proceedings of the IEEE/CVF conference on computer vision and pattern recognition*, pp. 8415–8424, 2021.
- Jacob Devlin, Ming-Wei Chang, Kenton Lee, and Kristina Toutanova. Bert: Pre-training of deep bidirectional transformers for language understanding. In *Proceedings of the 2019 conference of the North American chapter of the association for computational linguistics: human language technologies, volume 1 (long and short papers)*, pp. 4171–4186, 2019.
- Haiwen Diao, Ying Zhang, Lin Ma, and Huchuan Lu. Similarity reasoning and filtration for image-text matching. In *Proceedings of the AAAI conference on artificial intelligence*, volume 35, pp. 1218–1226, 2021.
- Alexey Dosovitskiy, Lucas Beyer, Alexander Kolesnikov, Dirk Weissenborn, Xiaohua Zhai, Thomas Unterthiner, Mostafa Dehghani, Matthias Minderer, Georg Heigold, Sylvain Gelly, et al. An image is worth 16x16 words: Transformers for image recognition at scale. *arXiv preprint arXiv:2010.11929*, 2020.
- Fartash Faghri, David J Fleet, Jamie Ryan Kiros, and Sanja Fidler. Vse++: Improving visual-semantic embeddings with hard negatives. *arXiv preprint arXiv:1707.05612*, 2017.
- Zheren Fu, Zhendong Mao, Yan Song, and Yongdong Zhang. Learning semantic relationship among instances for image-text matching. In *Proceedings of the IEEE/CVF Conference on Computer Vision and Pattern Recognition*, pp. 15159–15168, 2023.
- Zheren Fu, Lei Zhang, Hou Xia, and Zhendong Mao. Linguistic-aware patch slimming framework for fine-grained cross-modal alignment. In *Proceedings of the IEEE/CVF Conference on Computer Vision and Pattern Recognition*, pp. 26307–26316, 2024.
- Ross Girshick. Fast r-cnn. In *Proceedings of the IEEE international conference on computer vision*, pp. 1440–1448, 2015.

- Dalu Guo, Chang Xu, and Dacheng Tao. Image-question-answer synergistic network for visual dialog. In *Proceedings of the IEEE/CVF Conference on Computer Vision and Pattern Recognition*, pp. 10434–10443, 2019.
- Zhicheng Huang, Zhaoyang Zeng, Yupan Huang, Bei Liu, Dongmei Fu, and Jianlong Fu. Seeing out of the box: End-to-end pre-training for vision-language representation learning. In *Proceedings of the IEEE/CVF conference on computer vision and pattern recognition*, pp. 12976–12985, 2021.
- Wonjae Kim, Bokyoung Son, and Ildoo Kim. Vilt: Vision-and-language transformer without convolution or region supervision. In *International conference on machine learning*, pp. 5583–5594. PMLR, 2021.
- Kuang-Huei Lee, Xi Chen, Gang Hua, Houdong Hu, and Xiaodong He. Stacked cross attention for image-text matching. In *Proceedings of the European conference on computer vision (ECCV)*, pp. 201–216, 2018.
- Junnan Li, Ramprasaath Selvaraju, Akhilesh Gotmare, Shafiq Joty, Caiming Xiong, and Steven Chu Hong Hoi. Align before fuse: Vision and language representation learning with momentum distillation. *Advances in neural information processing systems*, 34:9694–9705, 2021.
- Junnan Li, Dongxu Li, Caiming Xiong, and Steven Hoi. Blip: Bootstrapping language-image pre-training for unified vision-language understanding and generation. In *International conference on machine learning*, pp. 12888–12900. PMLR, 2022.
- Sheng Li, Zhiqiang Tao, Kang Li, and Yun Fu. Visual to text: Survey of image and video captioning. *IEEE Transactions on Emerging Topics in Computational Intelligence*, 3(4):297–312, 2019.
- Tsung-Yi Lin, Michael Maire, Serge Belongie, James Hays, Pietro Perona, Deva Ramanan, Piotr Dollár, and C Lawrence Zitnick. Microsoft coco: Common objects in context. In *European conference on computer vision*, pp. 740–755. Springer, 2014.
- Haotian Liu, Chunyuan Li, Qingyang Wu, and Yong Jae Lee. Visual instruction tuning, 2023.
- Meizhen Liu, Anis Salwa Mohd Khairuddin, Khairunnisa Hasikin, and Weitong Liu. Novel cross-dimensional coarse-fine-grained complementary network for image-text matching. *PeerJ Computer Science*, 11:e2725, 2025a.
- Yang Liu, Wentao Feng, Zhuoyao Liu, Shudong Huang, and Jiancheng Lv. Aligning information capacity between vision and language via dense-to-sparse feature distillation for image-text matching. *arXiv preprint arXiv:2503.14953*, 2025b.
- Yang Liu, Mengyuan Liu, Shudong Huang, and Jiancheng Lv. Asymmetric visual semantic embedding framework for efficient vision-language alignment. In *Proceedings of the AAAI Conference on Artificial Intelligence*, volume 39, pp. 5676–5684, 2025c.
- Ze Liu, Yutong Lin, Yue Cao, Han Hu, Yixuan Wei, Zheng Zhang, Stephen Lin, and Baining Guo. Swin transformer: Hierarchical vision transformer using shifted windows. In *Proceedings of the IEEE/CVF international conference on computer vision*, pp. 10012–10022, 2021.
- Ilya Loshchilov and Frank Hutter. Decoupled weight decay regularization. *arXiv preprint arXiv:1711.05101*, 2017.
- Chris J Maddison, Andriy Mnih, and Yee Whye Teh. The concrete distribution: A continuous relaxation of discrete random variables. *arXiv preprint arXiv:1611.00712*, 2016.
- Lingchen Meng, Hengduo Li, Bor-Chun Chen, Shiyi Lan, Zuxuan Wu, Yu-Gang Jiang, and Ser-Nam Lim. Advait: Adaptive vision transformers for efficient image recognition. In *Proceedings of the IEEE/CVF conference on computer vision and pattern recognition*, pp. 12309–12318, 2022.
- Zhengxin Pan, Fangyu Wu, and Bailing Zhang. Fine-grained image-text matching by cross-modal hard aligning network. In *Proceedings of the IEEE/CVF conference on computer vision and pattern recognition*, pp. 19275–19284, 2023.

- Alec Radford, Jong Wook Kim, Chris Hallacy, Aditya Ramesh, Gabriel Goh, Sandhini Agarwal, Girish Sastry, Amanda Askell, Pamela Mishkin, Jack Clark, et al. Learning transferable visual models from natural language supervision. In *International conference on machine learning*, pp. 8748–8763. PmLR, 2021.
- Yongming Rao, Wenliang Zhao, Benlin Liu, Jiwen Lu, Jie Zhou, and Cho-Jui Hsieh. Dynamicvit: Efficient vision transformers with dynamic token sparsification. *Advances in neural information processing systems*, 34:13937–13949, 2021.
- Wei Wu, Kecheng Zheng, Shuailei Ma, Fan Lu, Yuxin Guo, Yifei Zhang, Wei Chen, Qingpei Guo, Yujun Shen, and Zheng-Jun Zha. Lotlip: Improving language-image pre-training for long text understanding. *Advances in Neural Information Processing Systems*, 37:64996–65019, 2024.
- Peter Young, Alice Lai, Micah Hodosh, and Julia Hockenmaier. From image descriptions to visual denotations: New similarity metrics for semantic inference over event descriptions. *Transactions of the association for computational linguistics*, 2:67–78, 2014.
- Beichen Zhang, Pan Zhang, Xiaoyi Dong, Yuhang Zang, and Jiaqi Wang. Long-clip: Unlocking the long-text capability of clip. In *European conference on computer vision*, pp. 310–325. Springer, 2024.
- Kun Zhang, Zhendong Mao, Quan Wang, and Yongdong Zhang. Negative-aware attention framework for image-text matching. In *Proceedings of the IEEE/CVF conference on computer vision and pattern recognition*, pp. 15661–15670, 2022.
- Zhuofan Zong, Kunchang Li, Guanglu Song, Yali Wang, Yu Qiao, Biao Leng, and Yu Liu. Self-slimmed vision transformer. In *European Conference on Computer Vision*, pp. 432–448. Springer, 2022.

Appendix to “SEPS: Semantic-enhanced Patch Slimming Framework for fine-grained cross-modal alignment”

In this appendix, we provide the following materials:

- A Comparison of VLP models on Flickr30K and MS-COCO (referring to Section 4.4 in the main paper);
- B Comparison of image-text retrieval performance for SEPS with different hyperparameters on Flickr30K (referring to Section 4.4 and Section 4.5 in the main paper);
- C Visualization of patch selection and alignment results.

A COMPARISON OF VLP MODELS ON FLICKR30K AND MS-COCO

To further validate the generalizability of our framework, we adapt SEPS to the widely-used CLIP pre-trained model, comparing it in Table 3 against both mainstream VLP models and prior fine-grained methods on the same backbone. While prior fine-grained methods like LAPS (Fu et al., 2024) demonstrate strong performance on the CLIP backbone, they do not consistently close the performance gap to leading VLP models such as BLIP (Li et al., 2022), particularly on the more challenging MS-COCO benchmark. In stark contrast, SEPS not only significantly surpasses all prior fine-grained methods but also successfully bridges this performance gap. Notably, in the text-to-image retrieval task on MS-COCO under the CLIP-Large backbone, SEPS achieves an R@1 score of 79.3%, which not only far surpasses the 57.1% from LAPS but also substantially outperforms the powerful BLIP model’s 63.1%. This result provides compelling evidence that our sophisticated dual-guidance mechanism is particularly effective in handling complex visual scenarios, establishing the competitive strength of SEPS even against large-scale, end-to-end pre-trained models.

Table 3: The comparisons of image-text retrieval for Vision-Language Pre-training (VLP) Models. *FG* indicates whether the method fine-grained alignment.

Method	<i>FG</i>	Flickr30K 1K				MS-COCO 5K			
		Image-to-Text R@1	Image-to-Text R@5	Text-to-Image R@1	Text-to-Image R@5	Image-to-Text R@1	Image-to-Text R@5	Text-to-Image R@1	Text-to-Image R@5
UNITER (Chen et al., 2019)	✓	87.3	98.0	75.6	94.1	65.7	88.6	52.9	79.9
VILT (Kim et al., 2021)	✓	83.5	96.7	64.4	88.7	61.5	86.3	42.7	72.9
SOHO (Huang et al., 2021)	✓	86.5	98.1	72.5	92.7	66.4	88.2	50.6	78.0
ALBEF (Li et al., 2021)	✓	<u>95.9</u>	99.8	<u>85.6</u>	97.5	<u>77.6</u>	<u>94.3</u>	<u>60.7</u>	<u>84.3</u>
BLIP (Li et al., 2022)	✓	96.6	99.8	87.2	97.5	80.6	95.2	63.1	85.3
<i>CLIP-ViT-Base-224 + CLIP-BERT-Base, 14 × 14 patches</i>									
CLIP (Radford et al., 2021)	✗	81.4	96.2	61.1	85.4	52.3	76.2	33.3	58.2
VSE++ (Faghri et al., 2017)	✗	92.2	<u>99.1</u>	80.5	<u>95.6</u>	68.0	88.2	53.6	79.7
SCAN (Lee et al., 2018)	✓	88.2	98.1	75.3	93.1	65.4	88.0	50.7	77.6
LAPS (Fu et al., 2024)	✓	<u>92.9</u>	99.3	<u>80.6</u>	95.5	<u>69.8</u>	<u>90.4</u>	<u>54.3</u>	<u>80.0</u>
SEPS	✓	94.7	97.6	93.1	97.7	84.1	91.2	78.4	95.5
<i>CLIP-ViT-Large-224 + CLIP-BERT-Large, 16 × 16 patches</i>									
CLIP (Radford et al., 2021)	✗	85.0	97.7	61.3	87.0	55.9	79.1	35.9	60.9
VSE++ (Faghri et al., 2017)	✗	94.0	<u>99.5</u>	83.4	96.4	68.5	89.4	56.7	81.9
SCAN (Lee et al., 2018)	✓	90.0	98.5	82.0	95.9	68.0	90.4	53.2	80.7
LAPS (Fu et al., 2024)	✓	<u>94.6</u>	99.9	<u>84.9</u>	<u>97.3</u>	<u>72.9</u>	91.7	<u>57.1</u>	<u>81.3</u>
SEPS	✓	95.8	98.4	95.1	98.1	86.5	91.7	79.3	95.8

B COMPARISON OF IMAGE-TEXT RETRIEVAL PERFORMANCE FOR SEPS WITH DIFFERENT HYPERPARAMETERS ON FLICKR30K.

Table 4: The comparisons of image-text retrieval for SEPS-ViT and SEPS-Swin with different selection ratio ρ on Flickr30K.

ρ	Image-to-Text			Text-to-Image			rSum
	R@1	R@5	R@10	R@1	R@5	R@10	
<i>ViT-Base-224 + BERT-base, 14×14 patches</i>							
0.1	85.6	91.9	97.0	85.1	97.0	98.6	553.4
0.2	86.5	92.4	96.6	86.3	97.5	98.9	557.3
0.3	87.4	92.9	96.2	87.5	98.0	99.2	561.2
0.4	87.0	94.2	97.0	87.1	98.3	99.3	562.8
0.5	86.5	95.4	97.8	86.6	98.6	99.4	564.3
0.6	87.0	94.1	97.3	86.9	98.3	99.2	562.8
0.7	87.5	92.8	96.8	87.3	97.9	99.0	561.3
0.8	86.9	92.6	96.4	86.8	97.9	99.1	559.8
0.9	86.2	92.5	96.1	86.3	97.8	99.2	558.2
<i>ViT-Base-384 + BERT-base, 24×24 patches</i>							
0.1	89.8	90.9	97.6	87.8	97.7	98.7	560.5
0.2	90.7	91.4	97.2	89.0	98.2	99.0	564.4
0.3	91.6	91.9	96.8	90.2	98.7	99.3	568.4
0.4	91.2	93.2	97.6	89.8	99.0	99.4	569.9
0.5	90.7	94.4	98.4	89.3	99.3	99.5	571.5
0.6	91.2	93.1	97.9	89.7	98.9	99.3	570.0
0.7	91.7	91.8	97.4	90.0	98.6	99.1	568.5
0.8	91.1	91.7	97.0	89.5	98.5	99.2	566.9
0.9	90.4	91.5	96.7	89.0	98.5	99.3	565.3
<i>Swin-Base-224 + BERT-base, 7×7 patches</i>							
0.1	89.8	96.8	98.6	86.8	98.7	99.5	569.2
0.2	90.2	97.2	98.7	87.3	98.8	99.6	571.8
0.3	90.4	96.6	98.6	87.0	98.8	99.5	570.8
0.4	90.5	96.4	98.5	86.9	98.8	99.5	570.6
0.5	90.7	96.8	98.7	87.8	98.9	99.6	572.4
0.6	90.8	97.1	98.8	88.5	98.9	99.7	573.8
0.7	90.2	97.0	98.7	88.2	98.9	99.6	572.6
0.8	89.8	96.9	98.7	88.0	98.9	99.6	572.0
0.9	89.5	96.5	98.6	87.5	98.8	99.5	570.9
<i>Swin-Base-384 + BERT-base, 12×12 patches</i>							
0.1	92.6	98.0	99.0	90.2	99.2	99.7	578.5
0.2	93.1	98.4	99.1	90.8	99.3	99.8	581.2
0.3	93.3	97.8	99.0	90.5	99.3	99.7	580.1
0.4	93.4	97.6	98.9	90.4	99.3	99.7	579.9
0.5	93.6	98.0	99.1	91.4	99.4	99.8	581.8
0.6	93.7	98.3	99.2	92.1	99.4	99.9	583.2
0.7	93.1	98.2	99.1	91.8	99.4	99.8	582.0
0.8	93.6	98.3	99.2	91.6	99.4	99.8	581.9
0.9	92.4	97.7	99.0	91.1	99.3	99.7	580.3

To comprehensively evaluate our model’s sensitivity and generality with respect to the key hyperparameter ρ , we conducted exhaustive experiments on both ViT and Swin backbones. The detailed results are presented in Table 4 and visually summarized in Figure 3. The analysis reveals both consistencies and notable distinctions in the performance trends across the two architectures. The ViT architecture exhibits a performance curve that is relatively sensitive to the value of ρ , where the rSum score reaches a distinct peak around $\rho = 0.5$ before declining at a comparatively rapid rate. In contrast, the Swin architecture demonstrates significant robustness; its performance curve maintains a near-peak level across a broad range of ρ from 0.2 to 0.8, without showing sharp degradation. This comparative analysis shows that while moderate information slimming is beneficial for both

Table 5: The comparisons of image-text retrieval for SEPS with different settings of coefficients on Flickr30K. The best results are marked **bold**.

λ_1	λ_2	Flickr30K 1K						rSum
		Image-to-Text			Text-to-Image			
		R@1	R@5	R@10	R@1	R@5	R@10	
0.25	0.25	85.8	94.3	97.8	83.1	97.6	98.7	557.4
0.25	0.5	85.0	92.9	96.6	85.0	97.5	98.7	555.7
0.25	0.75	84.7	92.4	96.2	85.6	97.7	98.9	555.5
0.25	1	84.8	86.9	94.0	83.2	97.0	98.7	544.6
0.5	0.25	86.8	96.7	97.9	85.5	97.9	99.1	563.9
0.5	0.5	86.5	95.4	97.8	86.6	98.6	99.4	564.3
0.5	0.75	85.6	91.2	95.7	86.1	97.7	99.0	555.3
0.5	1	86.6	92.5	96.9	86.3	98.3	99.3	559.9
1	0.25	85.3	96.9	98.9	69.7	93.0	97.0	540.9
1	0.5	86.4	94.7	98.1	86.7	98.3	99.4	563.7
1	0.75	86.0	94.5	97.1	87.3	98.2	99.3	562.4
1	1	86.1	93.7	96.9	86.9	98.1	99.2	560.9

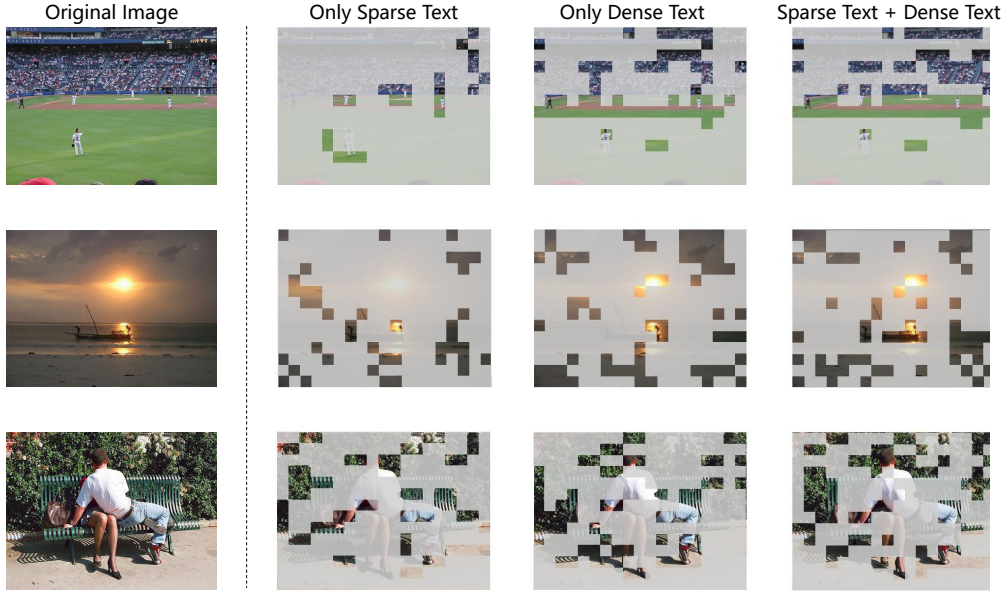


Figure 4: The visualization of visual patch selection with different combinations of sparse text and dense text.

backbones, our method possesses a very high tolerance for the choice of ρ on the Swin architecture. Overall, this provides compelling evidence for the universality and high stability of our proposed method, highlighting its ability to readily adapt to different mainstream visual backbones without requiring meticulous hyperparameter tuning.

We conducted a comprehensive sensitivity analysis on the loss coefficients λ_1 (sparse text) and λ_2 (dense text) to assess the robustness of our proposed SEPS framework. As demonstrated in Table 5, our model exhibits considerable stability across various coefficient combinations on the Flickr30K dataset. The overall performance metric rSum ranges from 540.9 to 564.3, representing a variation of approximately 4.2% relative to the optimal configuration, which underscores the model’s inherent robustness to hyperparameter selection. Notably, the optimal configuration ($\lambda_1 = 0.5, \lambda_2 = 0.5$) achieved the highest rSum of 564.3, demonstrating balanced performance across both retrieval directions. This configuration also yielded superior results in text-to-image retrieval, attaining R@5 and R@10 scores of 98.6% and 99.4%, respectively. Conversely, for image-to-text retrieval, the



Figure 5: The visualization of cross-modal alignment results of SEPS.

setting ($\lambda_1 = 0.5, \lambda_2 = 0.25$) achieved the highest R@1 performance of 86.8%, while the ($\lambda_1 = 1, \lambda_2 = 0.25$) configuration excelled in R@5 and R@10 metrics with scores of 96.9% and 98.9%, respectively. In the challenging text-to-image R@1 task, the ($\lambda_1 = 1, \lambda_2 = 0.75$) configuration delivered the peak performance of 87.3%. These results reveal that while individual metrics may favor specific coefficient combinations, the overall model maintains consistently high performance across the parameter space. This stability pattern strongly indicates that the superior performance of SEPS stems from its fundamental architectural design principles rather than from aggressive hyperparameter optimization, thus validating the effectiveness of our semantic guidance mechanism utilizing dense textual representations.

C VISUALIZATION

To intuitively illustrate the internal mechanism and final efficacy of our SEPS framework, we provide a qualitative visual analysis. Figure 4 clearly reveals the visual patch selection process. When guided solely by sparse text, the model identifies primary objects, but the selection can be coarse. Conversely, dense text alone can add detail but may sometimes overemphasize secondary regions. In contrast, our SEPS framework achieves a more precise selection of visual evidence by being the first to combine MLLM-generated dense text with original sparse captions. This combination allows the model to effectively bridge the information density gap between modalities, fusing the global context from sparse captions with the granular detail from dense descriptions to accurately preserve all semantically relevant patches. This superior patch selection capability translates directly into more robust fine-grained alignment, as demonstrated in Figure 5. Our model successfully aligns a single complex image with multiple, semantically diverse, yet correct captions, such as understanding both "Baseball players are playing" and "A crowd cheers on a baseball team." In summary, these visualizations intuitively demonstrate our core insight. By systematically leveraging dense text to assist visual patch selection, the SEPS framework achieves a more comprehensive scene understanding, which is the key to its state-of-the-art recall in complex fine-grained alignment tasks.